QUANTIFYING INSTABILITY SOURCES IN LIQUID ROCKET ENGINES

NAS8-00070
Final Report

Prepared for:

National Aeronautics and Space Administration
George C. Marshall Space Flight Center
Marshall Space Flight Center, AL 35812

Prepared by:

Richard C. Farmer
Gary C. Cheng

SECA, Inc.
Suite 201
3313 Bob Wallace Avenue
Huntsville, AL 35805

June 9, 2000

QUANTIFYING INSTABILITY SOURCES IN LIQUID ROCKET ENGINES

Introduction

An investigation to develop computational methodology to predict the effects of combusting flows on acoustic pressure oscillations in liquid rocket engines (LREs) was conducted. The methodology is intended to explain the causal physics of combustion driven acoustic resonances in LREs. A rigorous solution of the turbulent, multi-phase, multi-dimensional, transient mass, momentum, and energy conservation equations with combustion provides all of the information required to describe acoustic resonances in rocket engines. Ideally, a computational fluid dynamics (CFD) code would provide such a solution. However, real rocket engines are so geometrically complex and contain so many internal flow control devices that such solutions have not been produced. With current computer power, such solutions are becoming possible. This work is an initial attempt to predict the acoustic field in a simple, but typical, liquid rocket engine (LRE). Classically, acoustic phenomena are simulated by solving a Poisson equation for pressure by over simplifying the description of all other transport phenomena until such a solution is possible.

The approach used in this work was to perform a CFD analysis of the combustion process with sufficient temporal resolution to identify the pressure/combustion interactions. A test case was chosen, which contained the physical elements known to be important in influencing stability, for developing the required boundary conditions and physics for a CFD solution to be useful. The commonly used impinging type injector elements are a major source of instabilities and were considered to be essential in the chosen test case. Since liquid propellants cannot practically be pre-mixed, mixing in the combustion chamber must be described. The nozzle throat serves as a well defined downstream boundary condition. However, the upstream boundary condition must be specified at a point which precludes upstream travel of pressure waves. It is not feasible to choose a generic boundary condition because there are so many variations of the engine feed and injector systems. Rather a specific configuration was investigated for which test data are available to verify the solution. Unfortunately, a typical engine experiment which was geometrically simple enough to be attractive for CFD analyses was not found. The best compromise between accepting some geometric complexity while retaining impinging injectors and observing instability phenomena was determined to be one of the subscale, Fastrac gas generator combustors investigated by MSFC. This combustor and operating conditions were used as the CFD test case.

Analysis of a Fastrac Gas Generator Type Combustor

Data from a gas generator combustor tested in the Fastrac development which manifested longitudinal instabilities was provided by Rocker [1]. The exit flow was choked; the injector elements were triplets. This case (P315-97-04, 6/10/97) was chosen for our investigation. A further attractive feature of this combustor (See Figure 1) was that the injector elements were located with fairly good circumferential symmetry. Two rows of F-O-F triplet elements were used, and the two row pattern was repeated circumferentially around the injector faceplate. A small nitrogen flow was injected along the centerline. The feed streams were controlled by cavitating venturi meters about 14 feet upstream of the faceplate. Hence, the flow was

controlled by the feed system cavitating venturis and injector element orifices and by the combustor nozzle throat. To expedite this brief Phase I investigation, an analysis of the feed system was not performed. Also, the combustor flowfield was assumed to be axisymmetric. The propellants were LOX and RP-1. The operating conditions were such that the mixture ratio used was low enough to form only a small amount of soot. The approach used for the investigation was to simulate the unsteady case with low temporal resolution to obtain an essentially steady-state solution, then to increase the temporal resolution to reveal instability phenomena. The feed system flowfields were not sonic; therefore, the possibility of injector flow chamber flow coupling must be considered. However, for these Phase I analyses, only chamber flow was simulated.

The CFD code used in this study is the FDNS-RFV code. This code uses real fluid properties to represent the propellants, be they gaseous or liquid. Thus, the propellants enter the combustor as liquids, as they mix react and heat-up they become gases. The flowfield so predicted corresponds to a homogeneous spray combustion. The gases and liquids are modeled as being locally at the same temperature and pressure. The atomization and vaporization are thereby treated as being very fast processes. The mixing between the propellants is modeled with the turbulent viscosity submodel, which is the k-ϵ model. The vaporization could be treated as a finite-rate process and the turbulence mixing submodel could be modified, if test data to quantify these processes were available. The combustion submodel pyrolyzes the RP-1 to a C_2 intermediate which in turn combusts with oxygen to CO and H_2. The combustion is completed with the wet CO mechanism. Soot is also allowed to form and to burn. Details of this combustion model are given in Table 1 and Ref. [2]. The rate-equations in the combustion model were tuned to give good predictions of temperature, molecular weight, and soot concentrations which have been observed in gas generator experiments [3, 4]. Matching these parameters should give accurate predictions of sound speed in typical gas generator type environments.

To simulate the combustor flow as an axisymmetric flow the propellants were modeled as coming from narrow slits at the location of the injector faceplate orifices. The steady state CFD solution is obtained by specifying the inflow, estimating the remainder of the flowfield, and iterating until the exit flow equals the inflow. Test data for the chamber pressure and temperature were used to verify the solution. Since the specified initial flowfield is significantly different from the solution, large pressure waves are initially produced. These waves decrease in amplitude until the steady conditions are reached. The final phase of the solution produces a slow, monotonic approach to the final answer. The final solution is shown in Figure 2. The predicted chamber pressure was 465 psia, compared to the 470 psia measured value. The measured flowrate was 7.05 lb/s; that from the simulation was 6.87 lb/s. The predicted temperatures are very close to the measured values of 1545-1573°R. The predicted mean flow properties near the end of the chamber are shown in Table 2. For the predicted sound speed in the chamber and the chamber geometry, the first longitudinal mode would correspond to 798 Hz. Equilibrium chemistry, 1-dimensional solutions were also run for this test case. Two chemistry models were used, one with soot formation and one without. The case with soot formation indicated that 44 mole% soot was formed, the chamber sound speed was 2358 fps, and the corresponding 1L frequency was 1278 Hz, molecular weight was 26, the temperature was 2023 R, and the flowrate was 4.5 lb/s. The case without soot gave the chamber sound speed of 1571

Table 1a. Combustion Kinetic Models for RP-1/O_2

RP-1 → 6.2 C_2H_4 Rate = $AT^B exp\{-E/RT\}$ $[RP\text{-}1]^{0.5}$ A = 3.0117×10^{10} , B = 0, E/R = 2.523×10^4
$C_2H_4 + O_2 \rightarrow 2\ CO + 2\ H_2$ Rate = $AT^B exp\{-E/RT\}$ $[C_2H_4]^{0.5}$ $[O_2]^{1.0}$ A = 1.29×10^{15}, B = 1, E/R = 2.516×10^4
48 C_2H_4 → Soot + 84 H_2 Rate = $AT^B exp\{-E/RT\}$ $[C_2H_4]^{2.0}$ $[O_2 + \epsilon]^{-0.5}$ A = 5.1308×10^{12}, B = -2, E/R = 1.611×10^4, $\epsilon = 0.001\rho/M_{O_2}$ g-mole/cm^3 ***Soot is defined as $C_{96}H_{24}$, this approximation makes incipient soot particles the right size and maintains the right carbon-to-hydrogen ratio for soot.***

Table 1b. Combustion Kinetic Model for Wet CO

Reactions	A	B	E/R
$H_2 + O_2 \rightleftharpoons OH + OH$	1.7000E13	0	2.4070E4
$OH + H_2 \rightleftharpoons H_2O + H$	2.1900E13	0	2.5900E3
$OH + OH \rightleftharpoons O + H_2O$	6.0230E12	0	5.5000E2
$O + H_2 \rightleftharpoons H + OH$	1.8000E10	1.0	4.4800E3
$H + O_2 \rightleftharpoons O + OH$	1.2200E17	-0.91	8.3690E3
$M + O + H \rightleftharpoons OH + M$	1.0000E16	0	0
$M + O + O \rightleftharpoons O_2 + M$	2.5500E18	-1.0	5.9390E4
$M + H + H \rightleftharpoons H_2 + M$	5.0000E15	0	0
$M + H + OH \rightleftharpoons H_2O + M$	8.4000E21	-2.0	0
$CO + OH \rightleftharpoons H + CO_2$	4.0000E12	0	4.0300E3
$CO + O_2 \rightleftharpoons CO_2 + O$	3.0000E12	0	2.5000E4
$CO + O + M \rightleftharpoons CO_2 + M$	6.0000E13	0	0

Table 2. Flow Properties at the End of the Combustor from the Two-Phase Simulation Which Were Used to Define the Ideal Gas

Temperature (°R)		Molecular weight (lb_m/lb_{mole})		γ	Density (lb_m/ft^3)	Speed of Sound (ft/s)	
1680		41.97		1.09	1.106	1472.7	
Species Concentrations (mass fractions)							
H_2O	CO	CO_2	H_2	C_2H_4	RP-1	Soot	N_2
0.063	0.2087	0.0419	0.0121	0.0705	0.5869	0.0162	0.0007

fps, the corresponding 1L frequency was 852 Hz, molecular weight was 21, the temperature was 1134 R, and the flowrate was 6.9 lb/s. The observed IL frequencies varied from 789 to 821 Hz. The assumption of equilibrium soot production is obviously poor. The CEC solution without soot production provides a reasonable estimate of the mass flowrate, but the predicted temperature and molecular weight differences between the CEC equilibrium and CFD solutions are significant. The equilibrium analysis pyrolyzes all of the hydrocarbons to small species. This is an endothermic process which cools the flow. The CFD analysis leaves much of the unreacted hydrocarbons present as vaporized RP-1. The presence of the RP-1 is necessary to match the mean molecular weights reported for gas generator tests [3]. Therefore, the finite-rate combustion model used in the CFD code is believed to offer the best estimate of flow properties in the Fastrack gas generator. Furthermore, the properties shown in Table 2 provides a good estimate of an ideal gas surrogate to represent the combusting propellants.

Transient Engine Simulations - Real Fluids

The plan was to continue the steady-state analysis with the code tuned to represent time accurate solutions using the real fluids option of the CFD code. First, the unsteady flowfield solution behavior was investigated by reducing the time-step size and using the implicit time integration option and continuing the calculation from the steady-state solution. Figure 3 shows the results of this simulation. As expected when the smaller time step and the implicit integration scheme are used, a perturbation resulted in the flow. This perturbation is seen to damp out and produce another steady-state answer which differs slightly from the solution shown in Figure 2. Such behavior suggests that the observed instability was due to coupling with the feed system and/or injector element orifice flows. Since the real fluids simulation is computationally intensive, it was deemed impractical to extend the computational domain upstream to the cavitating venturi meters in this short Phase I investigation. Rather, the inlet flow rate was perturbed in a sinusoidal manner to determine how the pressure field would develop. This forced perturbation crudely represents what would happen due to feed system/injector created flow disturbances. Figure 4 shows that the pressure (at the impingement point, #1) initially responds out of phase with the flowrate oscillation, and eventually becomes in phase with flowrate after several cycles of oscillation. Pressure monitoring station #3 is at the pressure measurement station which is about 3/4 of the way down the barrel section of the combustor, while station #2 is located between the turbulence ring and station #3. The pressure oscillations at the 2nd and 3rd monitoring stations become out of phase with those at the inlet

after the oscillations become regular. All of the pressure oscillations tend to become small in amplitude, i.e. about 5 psia. To determine if the pressure oscillations would continue after the flowrate/pressure at the inlet boundary was set to an empirical correlation, the simulation was continued with this boundary condition. This correlation will be described in the next section. Figure 5 shows that the simulation tends to diverge, but it took an excessive amount of clock time to make this determination. In fact so much time, that the correlation could not be tuned to obtain reasonable parameters in the correlation. Two other factors could also be causing pressure oscillation damping: (1) the simulation could be over damped by the turbulence model and/or the artificial (numerical) damping in the solver, and (2) the boundary conditions used to in the chamber. Such factors could only be evaluated parametrically. However, again due to the short time frame of the Phase I investigation, the real fluids CFD code required too much time to provide parametric studies of these effects. Therefore, these effects were studied with an ideal gas model to represent the chamber flow.

Transient Engine Simulations - Ideal Gases

In order to determine the cause of the pressure oscillation damping in the two-phase, real fluid combustion flow simulation, a series of transient, ideal-gas simulations was conducted. The propellants entering the combustion chamber were assumed to be premixed and pre-combusted and have the same flow properties as the mean flow at the end of the combustion chamber in the two-phase flow calculation. These flow properties are listed in Table 2. As previously noted, the temperature, mean molecular weight, and sound speed of the pre-combusted gas has a nature frequency which is close to the 1-L mode of the pressure oscillation in the Fastrac Gas Generator. Observing from Figure 2 that the hot-gas exit flow is representative of a large part of the combustor flow, the ideal-gas simulations should have approximately the same residence time in the combustor as the real gases.

The purpose of using the ideal-gas flow simulation to study the instability is to substantially reduce the computation time, such that various boundary conditions and numerical schemes can be tested in a timely fashion. In addition, the premixed, hot-gas flow simulation excludes the effects of combustion instability and spray/atomization/mixing instability, and thus the chamber pressure oscillations are due to acoustic waves only.

A steady-state calculation with a uniform profile of flow properties at the chamber inlet was performed first to establish a converged flow solution for the chamber and nozzle. The time history of the chamber pressure is plotted as shown in Figure 6. In the next step, the inlet hot-gas mass flow rate was perturbed according to the following function:

$$\dot{m} = \dot{m}_0 [\, 1 + \phi_m \sin (2\pi \omega_m t) \,]$$

where ϕ_m=0.3 and ω_m = 1/800 sec^{-1} were tuned to establish a 35 psi ($\Delta p/p_c \approx 0.074$) pressure oscillation at the inlet with a frequency of 800 Hz. Numerical calculations with perturbed inlet mass flow rates were conducted for more than 10 cycles. The numerical results indicated that the magnitude of pressure oscillations near the chamber exit were smaller than those at the inlet. To insure that the attenuation of the pressure oscillation was not caused by numerical damping and the over-prediction of the eddy viscosity, this ideal-gas simulation was repeated with: (1)

lower inlet turbulence intensity, (2) the temperature-corrected turbulence model, and (3) the exclusion of artificial damping terms in the FDNS-RFV code. The numerical results still indicated that both the mean pressure and the magnitude of pressure fluctuations vary along the streamwise locations, as shown in Figure 7. The location of Pressure #1 corresponds to the impingement point in the two-phase, spray calculation. The location of the pressure measurement near the chamber exit is identified as Pressure #3; while Pressure #2 is located between the turbulence ring and the location of Pressure #3. The predicted mean pressure is consistent with flow physics: highest pressure and lowest mean velocity at the chamber inlet; lowest pressure and highest mean velocity at Pressure #2 where recirculation zone behind the turbulence ring reduces the mean flow area; lower pressure and higher mean velocity at Pressure #3 which is near the end of the flow recirculation zone. These velocity and pressure fields are shown in Figure 8. It is to be noted that the phase lag between different pressure points remains constant, which indicates the implicit time integration scheme employed by the flow solver is accurate. Furthermore, the pressure at the impingement point, which is very close to the inlet, oscillates almost in phase with the inlet mass flow rate. Since the predicted eddy viscosity is believed to be small enough (the reattachment length behind the turbulence ring is longer than 8 step heights of the turbulence ring), the loss due to the viscous force should be small. Hence, the reduction of the chamber pressure and its fluctuations should be real phenomena. The most telling evidence that the variation in the chamber pressure amplitudes with location is real is that the smallest amplitude is at station #2. If the amplitude variation were due to dissipation only, the amplitudes could not decease to a minimum and then increase along the combustor. These observations suggest that relatively minor geometric complexities can have a profound influence on pressure waves in liquid rocket engines.

Several transient calculations were performed by starting with the predicted perturbed flowfield and by not using the inlet mass flowrate perturbation. Since the numerical calculations started at the injector face, the effects of upstream pressure/mass flux perturbations from either the injector orifices or the feed lines were not simulated. Numerical experiments were conducted to find a set of inlet boundary conditions, with which the chamber pressure fluctuations dissipated the least and the mean chamber pressure at specific locations remained constant during the transient numerical calculations. The inlet boundary condition for the static pressure is either zero gradient or constant gradient. There are four types of inlet boundary conditions for the velocity: constant mass flow rate, constant total pressure, constant velocity, and a correlation of the inlet mass flowrate fluctuation to the inlet pressure fluctuation which can be expressed as,

$$\frac{\Delta \dot{m}}{\dot{m}} = \phi_p \frac{\Delta p}{p_0}$$

ϕ_p is a constant tuned to meet the goal mentioned above. It was found that the constant pressure gradient boundary condition combined with any of the other velocity boundary conditions tends to overshoot or undershoot the mean chamber pressure. For example, see Figure 9. In addition, the pressure oscillations at various locations were damped out with time. The combination of zero pressure gradient with the correlation of mass flux fluctuation to the pressure fluctuation showed a larger variation in the numerical results for different values of ϕ_p. For negative ϕ_p (-5 and -1) where the oscillations of inlet mass flow rate are opposite to the oscillations of the inlet pressure, not only the mean pressure is lower but also the pressure

fluctuations decay faster compared to the results of positive ϕ_p, as shown in Figures 10 and 11, respectively. Moreover, the pressure fluctuations predicted with ϕ_p=-5 decay faster than those predicted with ϕ_p=-1. For positive ϕ_p (5 and 1) where the oscillations of inlet mass flow rate are in phase with the inlet pressure oscillations, the pressure fluctuations also decay but with a slower rate, see Figures 12 and 13. However, the mean pressures at various locations diverge if ϕ_p=5; but the mean values remain constant if ϕ_p=1. The combination of zero pressure gradient with constant inlet total pressure produced a high frequency mass flux fluctuation, still the pressure oscillation decayed very fast, as shown in Figure 14. The zero pressure gradient boundary condition in combination with either constant inlet velocity or constant inlet mass flux displayed the same characteristics as can be seen in Figures 15 and 16, respectively. Mean pressure at a given location remains constant with time, and the pressure fluctuations decreases with time. It should be noted that the decay of pressure fluctuations predicted by the combination of zero pressure gradient and constant inlet mass flux is the slowest compared to the other sets of inlet boundary conditions.

Based on these simulations, it is concluded that the combustion chamber and the nozzle will not be able to sustain instabilities. Since the pressure perturbations decrease along the streamwise direction due to the viscous and turbulence effects and the complex flowfield which exists in the chamber, smaller pressure waves return to the inlet boundary from the nozzle, and subsequently these pressure waves damp out. By examining the pressure test data, the pressure waves seem to exhibit a behavior such that the pressure oscillations decay for 3 cycles and are followed by a pressure spike. This characteristic is repeatable throughout the test data. It is suspected that there is a long-wave perturbation from upstream (feed line and/or injector orifices) which maintains the instability. It is further concluded that the observed instabilities in this Fastrack gas generator configuration are due to coupling between the feed line and/or injector element orifice flow coupling and the combustor flow proper. Further computational analyses should include a domain which extends through the injector orifice and to the cavitating venturis. The combustion physics included in the two-phase, real-fluid combustion models in the FDNS-RFV code should be used for these simulations even though they are time consuming to perform.

Conclusions and Recommendations

1. Real fluid CFD simulations of combustion stability phenomena in LREs are very computationally intensive, and should be addressed with the fastest processors available.

2. The rapid flowfield damping of real and ideal gas simulations of Fastrack type gas generators indicates that there is strong coupling between the feed line/injector element flowfields and those flowfields in the combustion chamber.

3. Unnecessary artificial damping in the FDNS-RFV code has been eliminated to expedite combustion stability simulations.

4. Numerous methods of applying chamber boundary conditions which were investigated did not significantly affect the dissipation of the perturbed solution to a steady or no-flow condition. Some of the boundary condition specifications considered caused an immediate computational instability to occur.

5. Oscillatory flows driven by chamber boundary condition specifications were shown to be modulated and for pressure waves to form because of local flowfield variations. Such variations are due to configuration variations as well as flow dissipation.

6. Future CFD stability analyses of Fastrack type gas generator combustors should be conducted for a computation region which includes flow control devices on both the in-flow and out-flow boundaries of the region. In-flow controls may be of the cavitating venturi type and out-flow, sonic throats of the nozzle.

7. Parallel processing on multiple PC processors should be used to provide the computer power needed to more completely address combustion stability issues of liquid rocket engines.

References

1. Rocker, M., "Data Review - Fastrac 60K Gas Generator," presentation, June 20, 1997.

2. Farmer, R., et al, "A Design Tool for Liquid Rocket Engine Injectors," AIAA 2000-3499, 36th AIAA/ASME/SAE/ASEE Joint Propulsion Conference, Huntsville, AL, 26-29 July 2000.

3. Hernandez, R., "Carbon Deposition Model for Oxygen-Hydrocarbon Combustion," RPT/AA0631-a/087, Aerojet TechSystems Co., Sacramento, CA, Sept. 1987.

4. Johnson, C., et al, "Prediction of Soot Production in Kerosene Fueled Liquid Rocket Engines," JANNAF 35th Combustion Subcommittee, Tucson, AZ, 1998.

Figure 1

60K Fastrac Gas Generator: Development Configuration 1

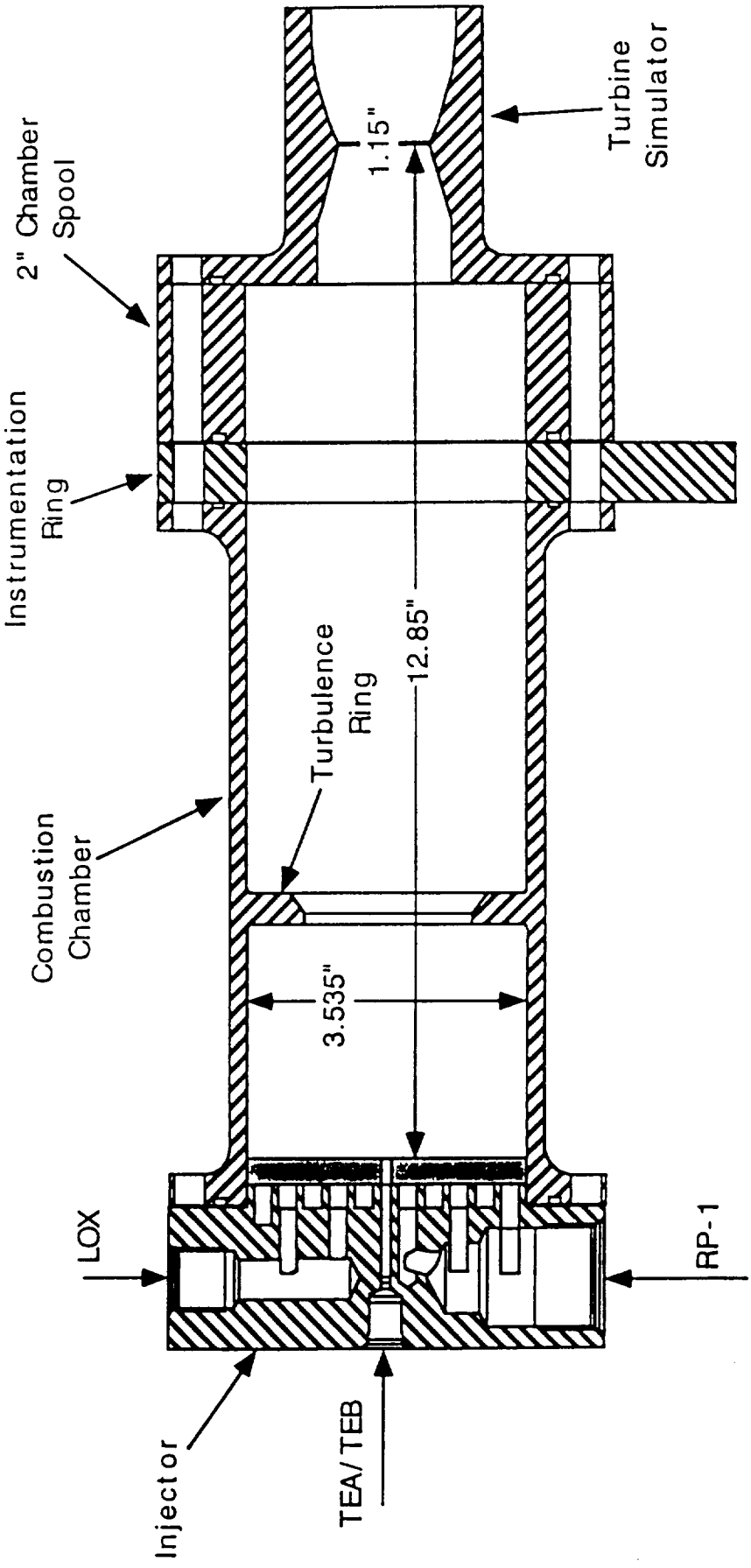

Figure 2

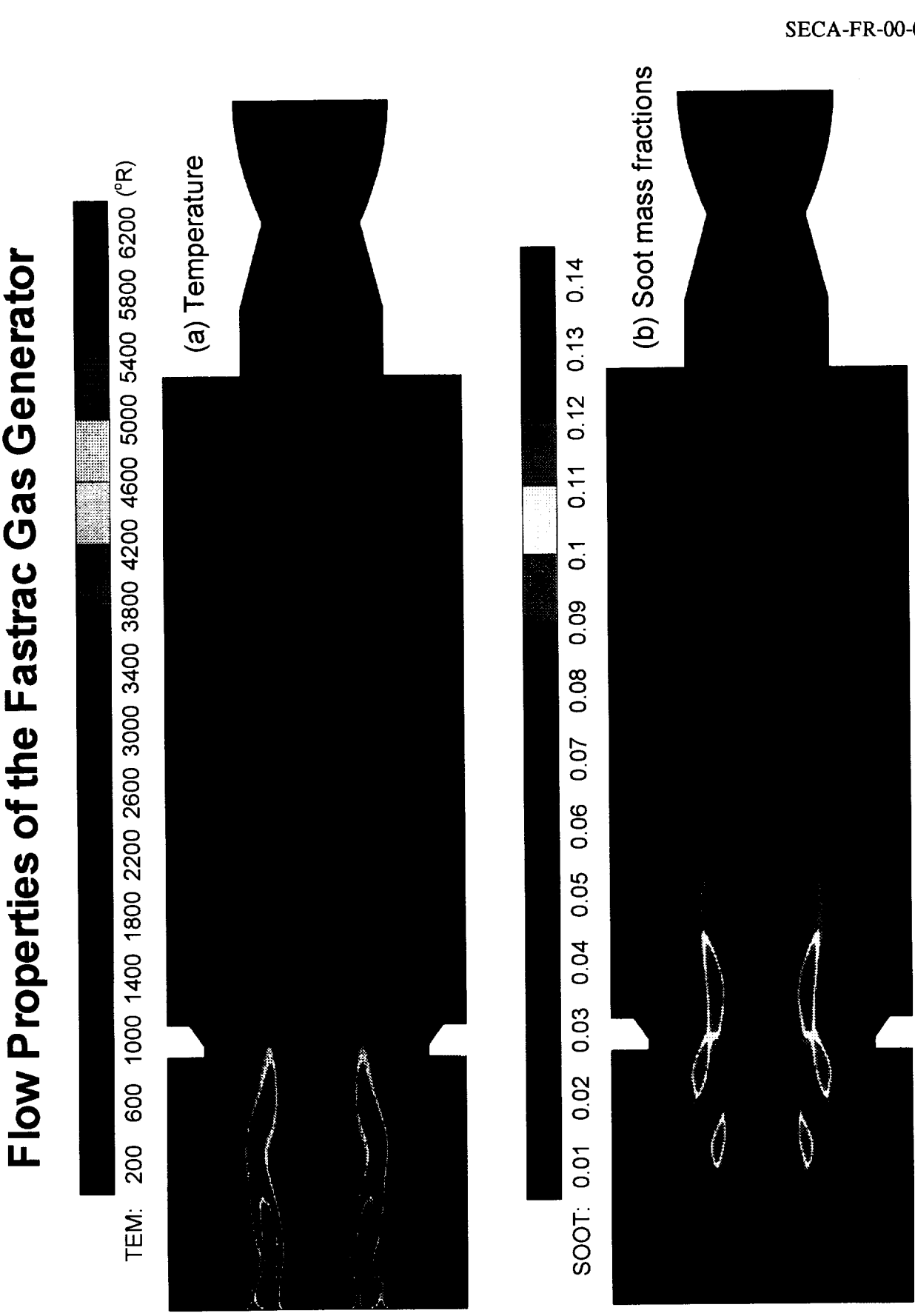
Flow Properties of the Fastrac Gas Generator
TEM: 200 600 1000 1400 1800 2200 2600 3000 3400 3800 4200 4600 5000 5400 5800 6200 (°R)
(a) Temperature
SOOT: 0.01 0.02 0.03 0.04 0.05 0.06 0.07 0.08 0.09 0.1 0.11 0.12 0.13 0.14
(b) Soot mass fractions

Figure 3

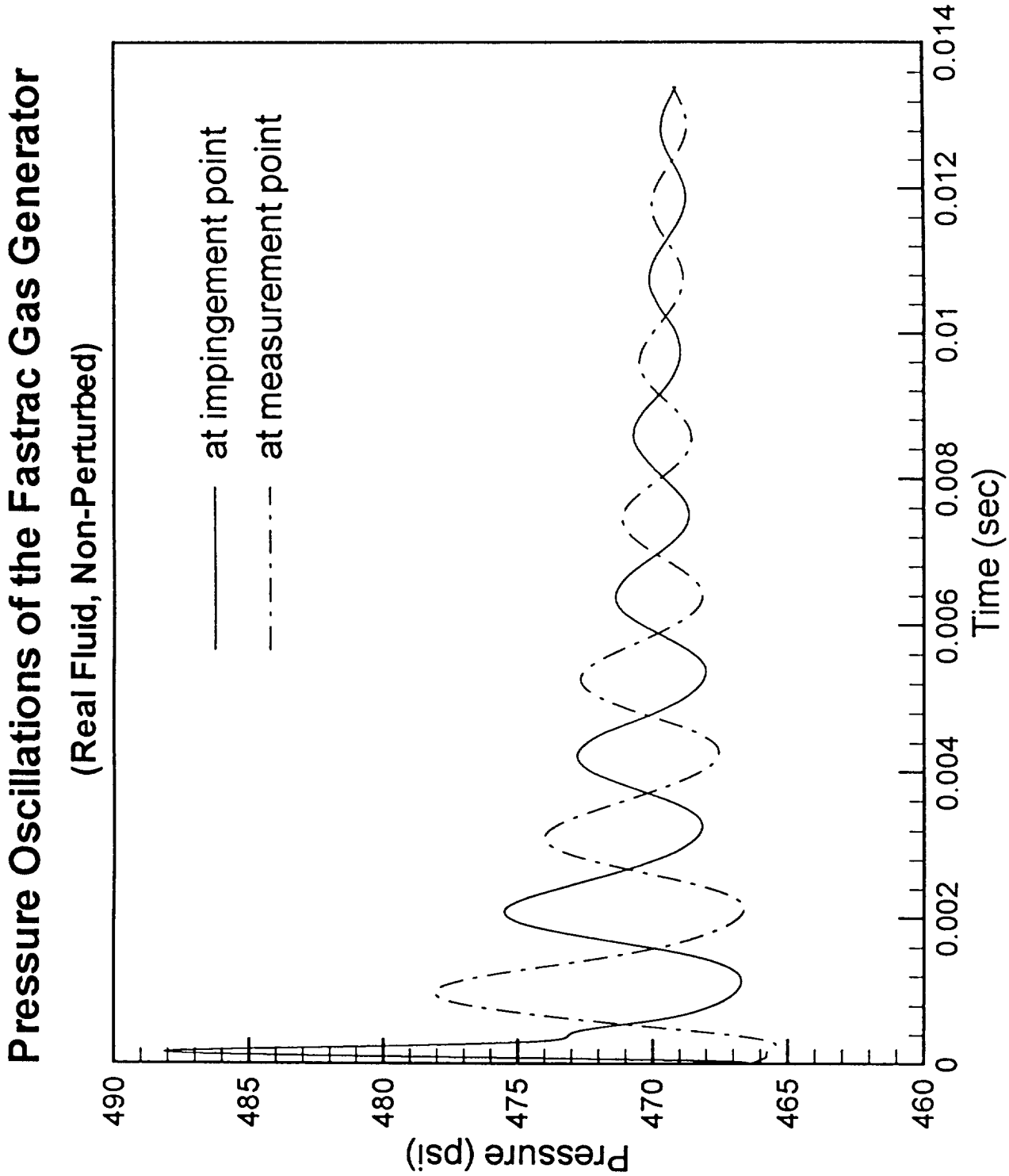
Pressure Oscillations of the Fastrac Gas Generator
(Real Fluid, Non-Perturbed)
at impingement point
at measurement point
Pressure (psi)
Time (sec)
490
485
480
475
470
465
460
0
0.002
0.004
0.006
0.008
0.01
0.012
0.014

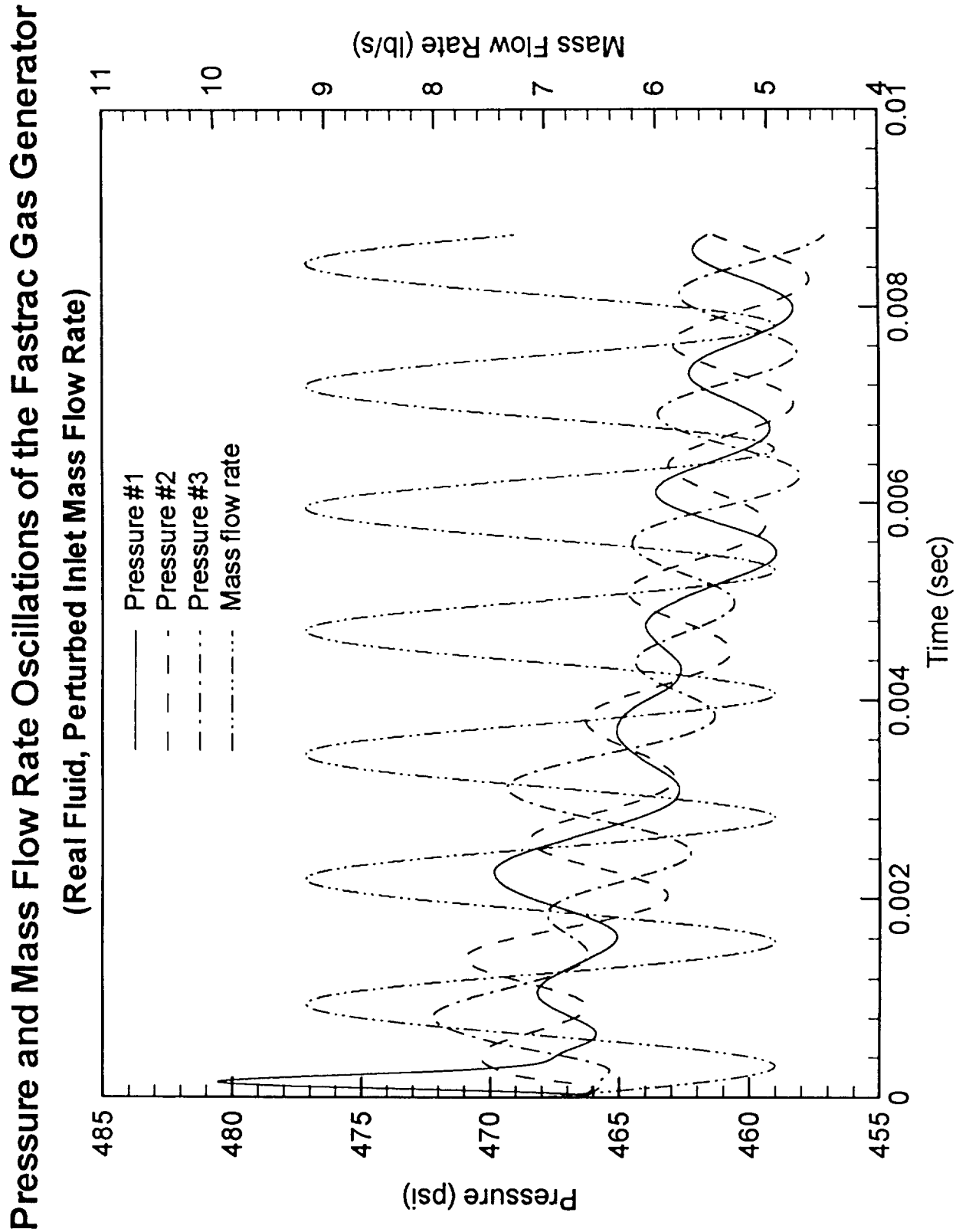
Pressure and Mass Flow Rate Oscillations of the Fastrac Gas Generator
(Real Fluid, Perturbed Inlet Mass Flow Rate)
Pressure #1
Pressure #2
Pressure #3
Mass flow rate
Pressure (psi)
Mass Flow Rate (lb/s)
Time (sec)
485
480
475
470
465
460
455
11
10
9
8
7
6
5
4
0
0.002
0.004
0.006
0.008
0.01

Figure 4

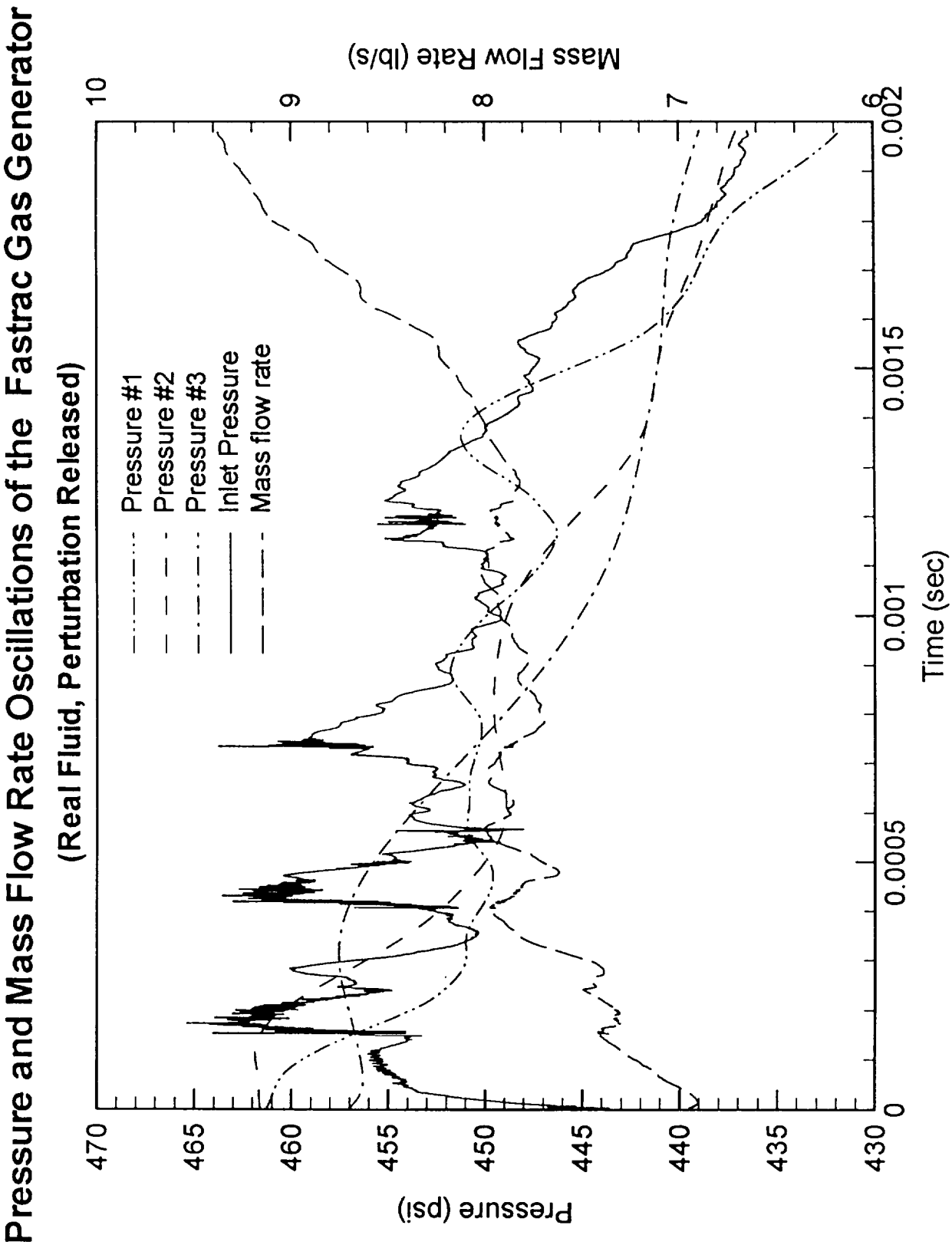
Pressure and Mass Flow Rate Oscillations of the Fastrac Gas Generator
(Real Fluid, Perturbation Released)
Pressure #1
Pressure #2
Pressure #3
Inlet Pressure
Mass flow rate
Pressure (psi)
Mass Flow Rate (lb/s)
Time (sec)
470
465
460
455
450
445
440
435
430
10
9
8
7
6
0
0.0005
0.001
0.0015
0.002

Figure 5

Figure 6

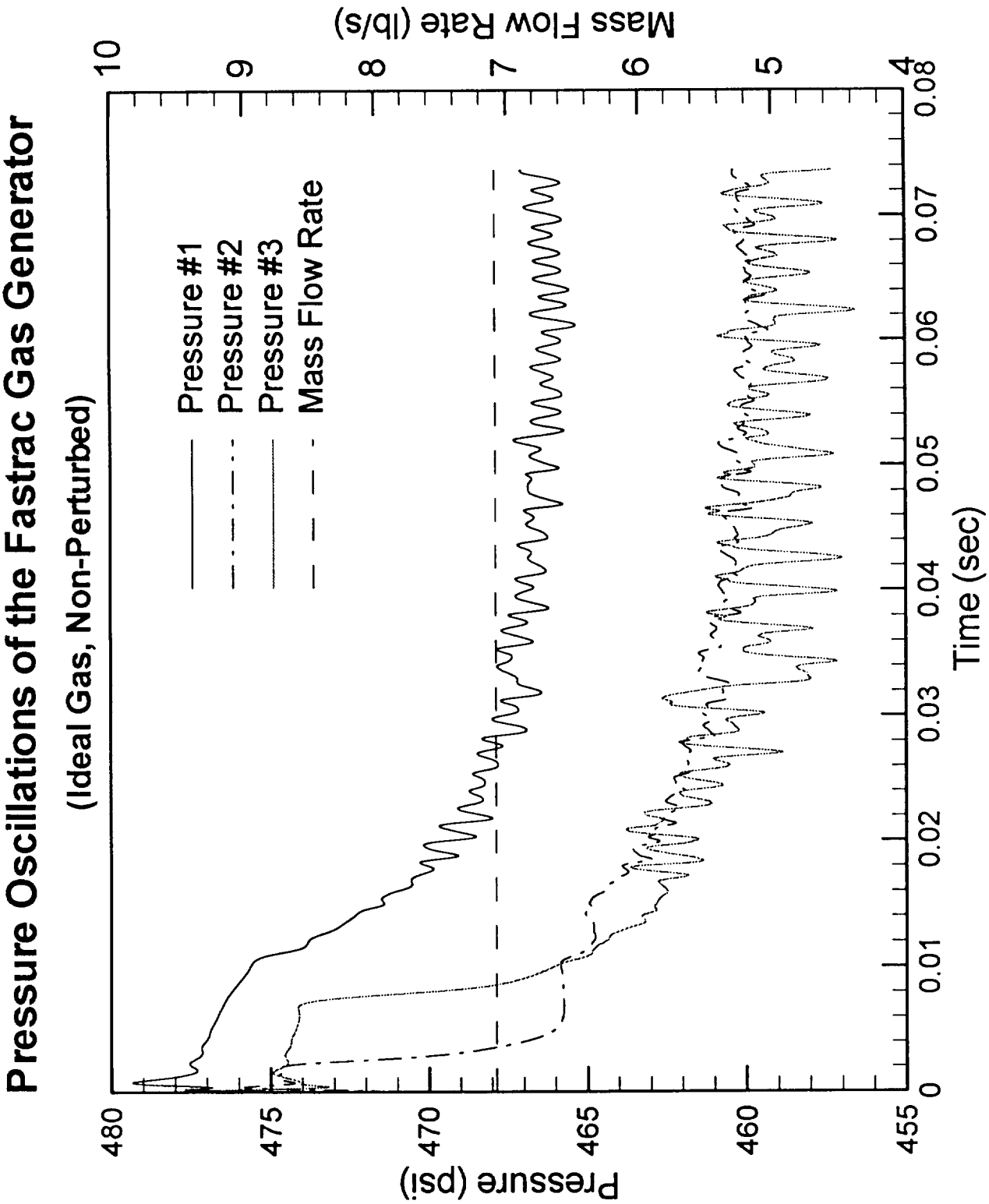
Pressure Oscillations of the Fastrac Gas Generator
(Ideal Gas, Non-Perturbed)
Pressure #1
Pressure #2
Pressure #3
Mass Flow Rate
Pressure (psi)
Mass Flow Rate (lb/s)
Time (sec)
480
475
470
465
460
455
10
9
8
7
6
5
4
0
0.01
0.02
0.03
0.04
0.05
0.06
0.07
0.08

Figure 7

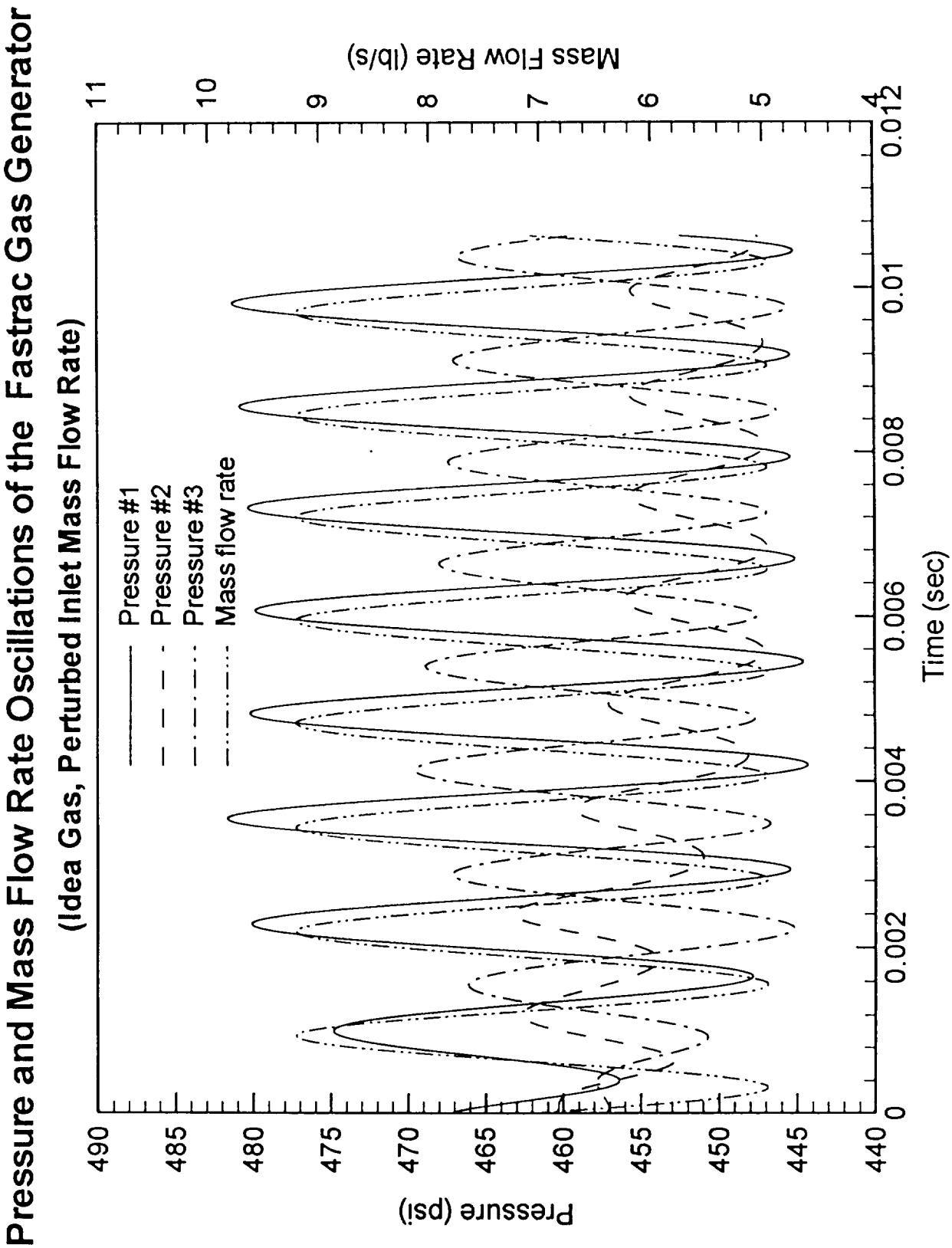
Pressure and Mass Flow Rate Oscillations of the Fastrac Gas Generator
(Idea Gas, Perturbed Inlet Mass Flow Rate)
Pressure #1
Pressure #2
Pressure #3
Mass flow rate
Pressure (psi)
Mass Flow Rate (lb/s)
Time (sec)
490
485
480
475
470
465
460
455
450
445
440
11
10
9
8
7
6
5
4
0
0.002
0.004
0.006
0.008
0.01
0.012

Figure 8

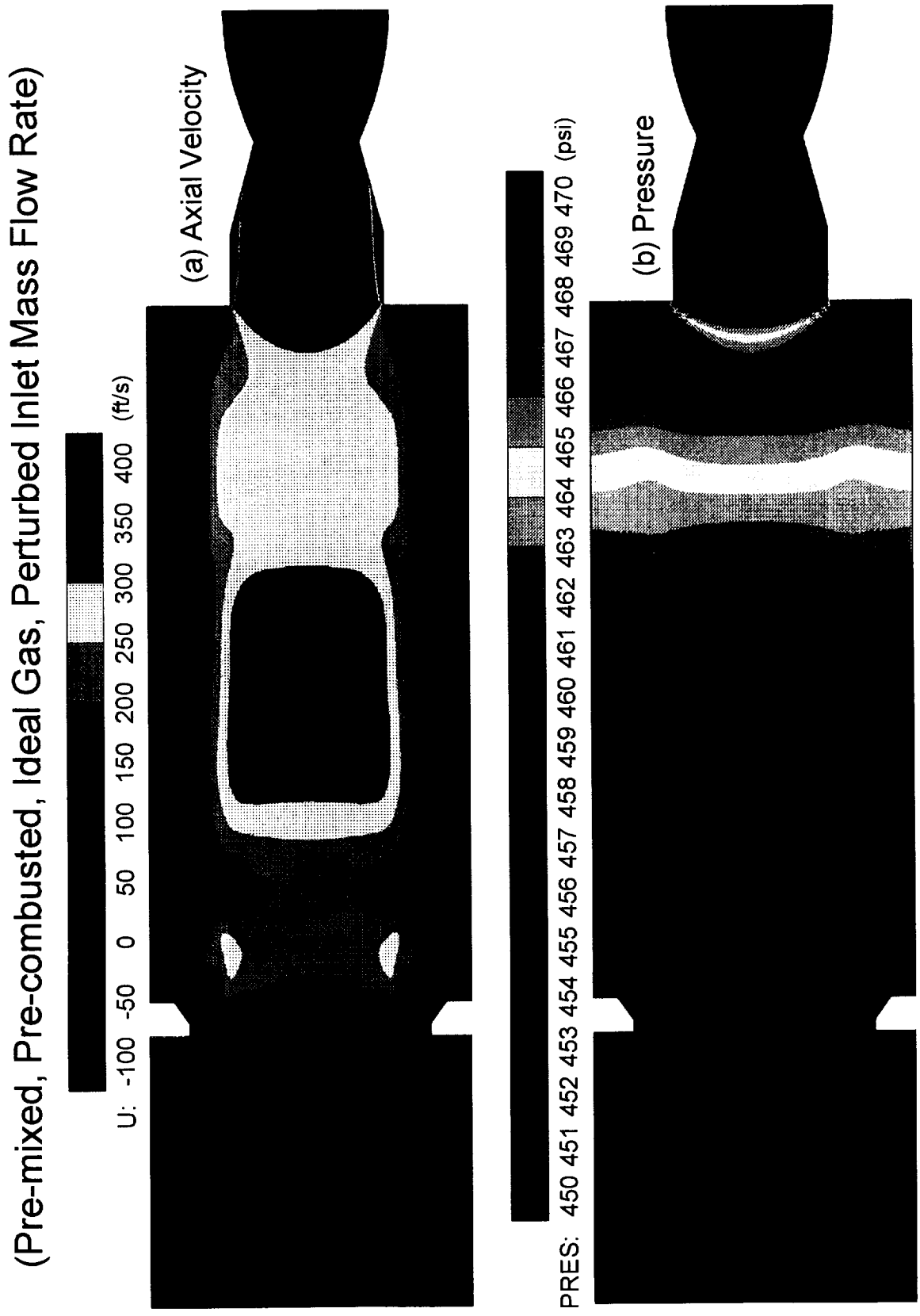
Flow Properties of the Fastrac Gas Generator
(Pre-mixed, Pre-combusted, Ideal Gas, Perturbed Inlet Mass Flow Rate)
(a) Axial Velocity
U: -100 -50 0 50 100 150 200 250 300 350 400 (ft/s)
(b) Pressure
PRES: 450 451 452 453 454 455 456 457 458 459 460 461 462 463 464 465 466 467 468 469 470 (psi)

Figure 9

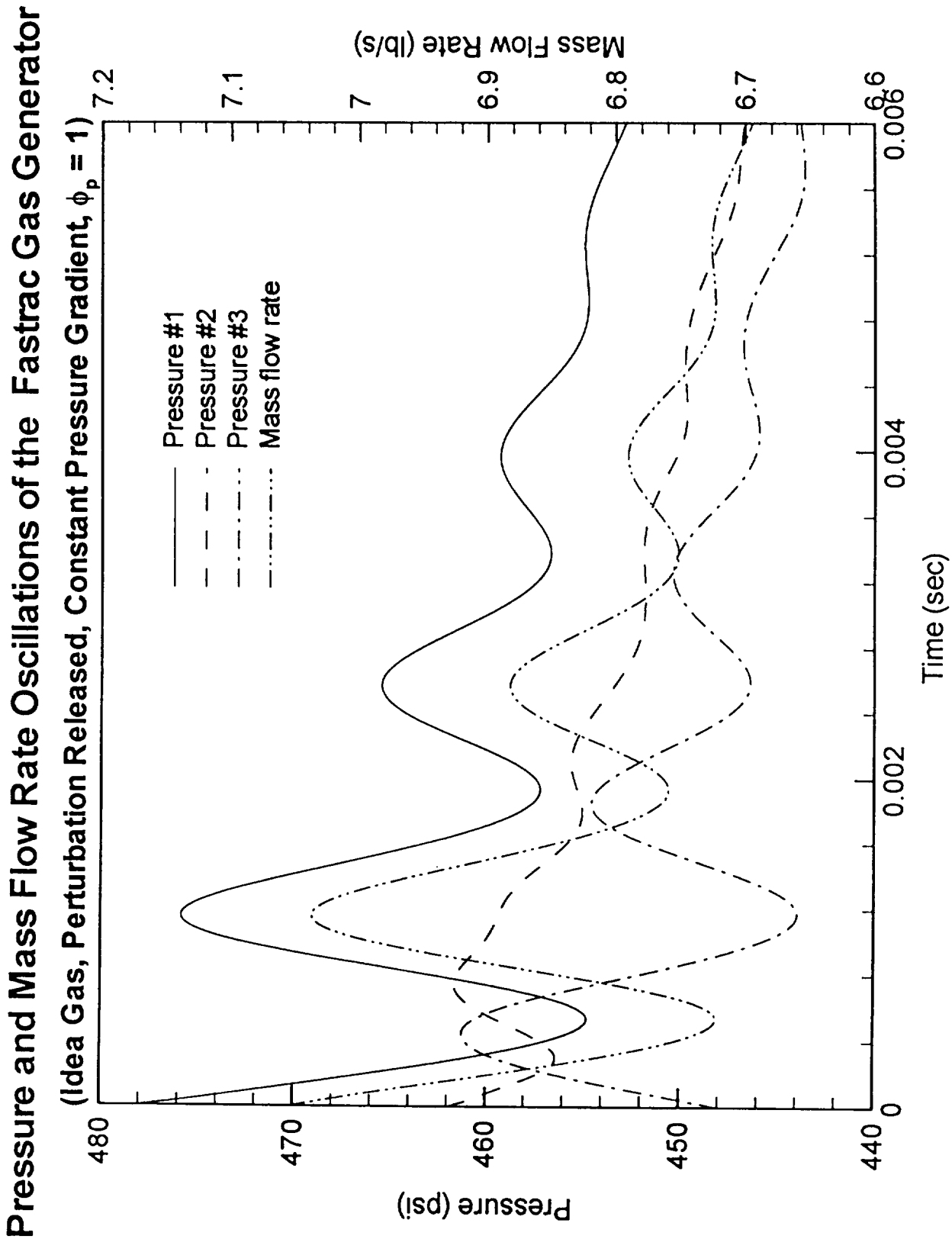
Pressure and Mass Flow Rate Oscillations of the Fastrac Gas Generator
(Idea Gas, Perturbation Released, Constant Pressure Gradient, ϕ_p = 1)
Pressure #1
Pressure #2
Pressure #3
Mass flow rate
Pressure (psi)
Mass Flow Rate (lb/s)
Time (sec)
480
470
460
450
440
7.2
7.1
7
6.9
6.8
6.7
6.6
0
0.002
0.004
0.006

Figure 10

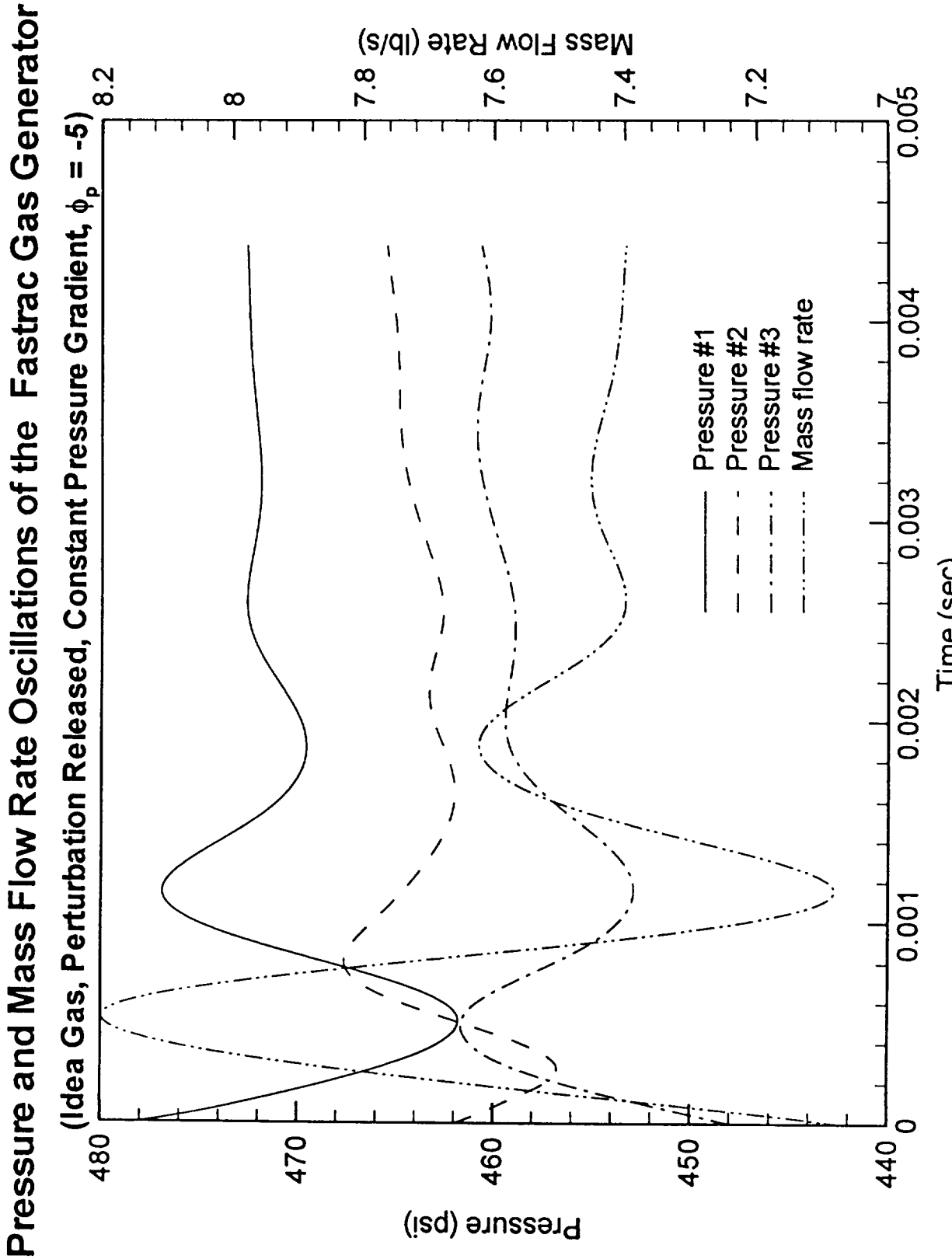
Pressure and Mass Flow Rate Oscillations of the Fastrac Gas Generator
(Idea Gas, Perturbation Released, Constant Pressure Gradient, ϕ_p = -5)
Pressure (psi)
Mass Flow Rate (lb/s)
Time (sec)
Pressure #1
Pressure #2
Pressure #3
Mass flow rate
480
470
460
450
440
8.2
8
7.8
7.6
7.4
7.2
7
0
0.001
0.002
0.003
0.004
0.005

Figure 11

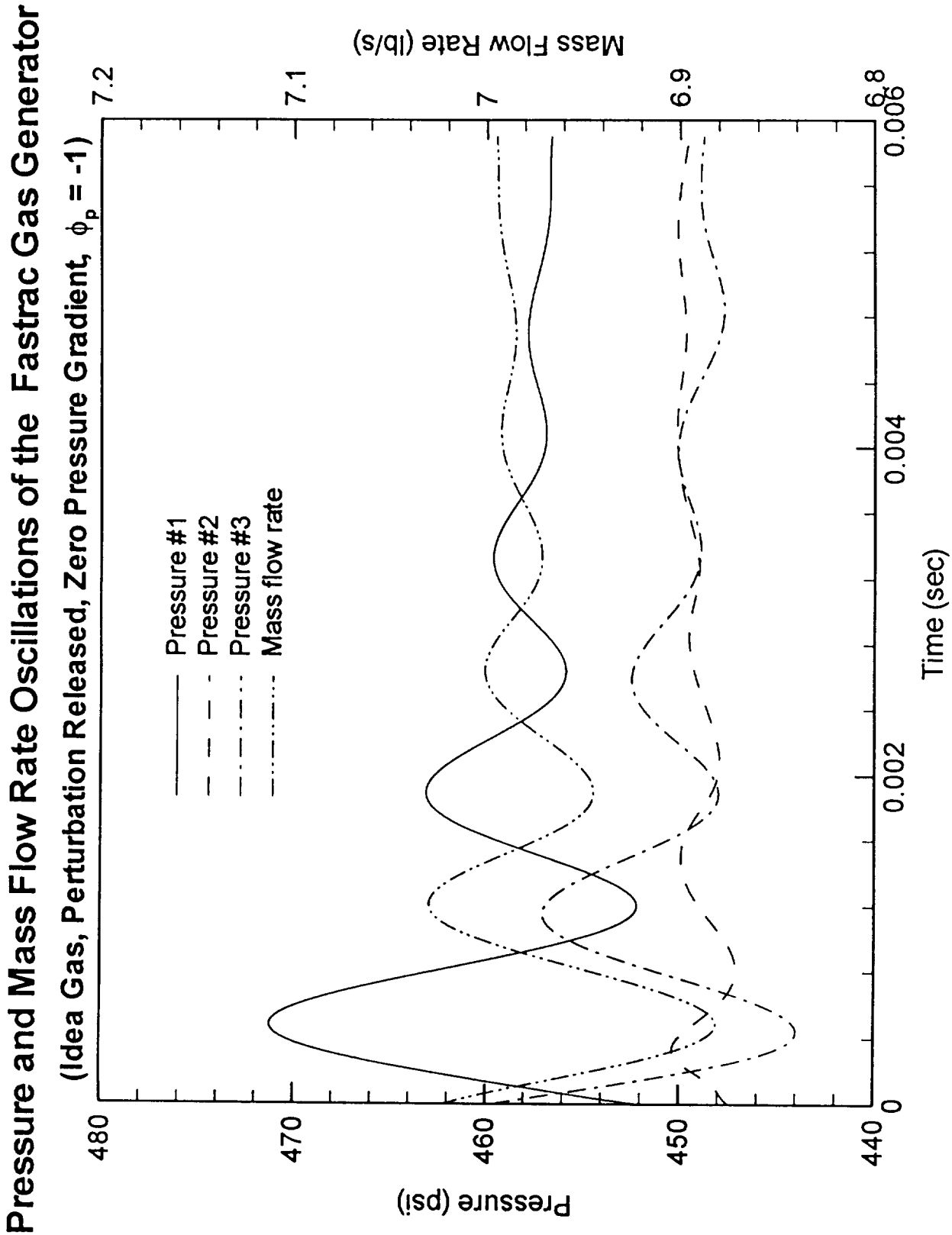
Pressure and Mass Flow Rate Oscillations of the Fastrac Gas Generator
(Idea Gas, Perturbation Released, Zero Pressure Gradient, ϕ_p = -1)
Pressure #1
Pressure #2
Pressure #3
Mass flow rate
Pressure (psi)
Mass Flow Rate (lb/s)
Time (sec)
480
470
460
450
440
7.2
7.1
7
6.9
6.8
0
0.002
0.004
0.006

Figure 12

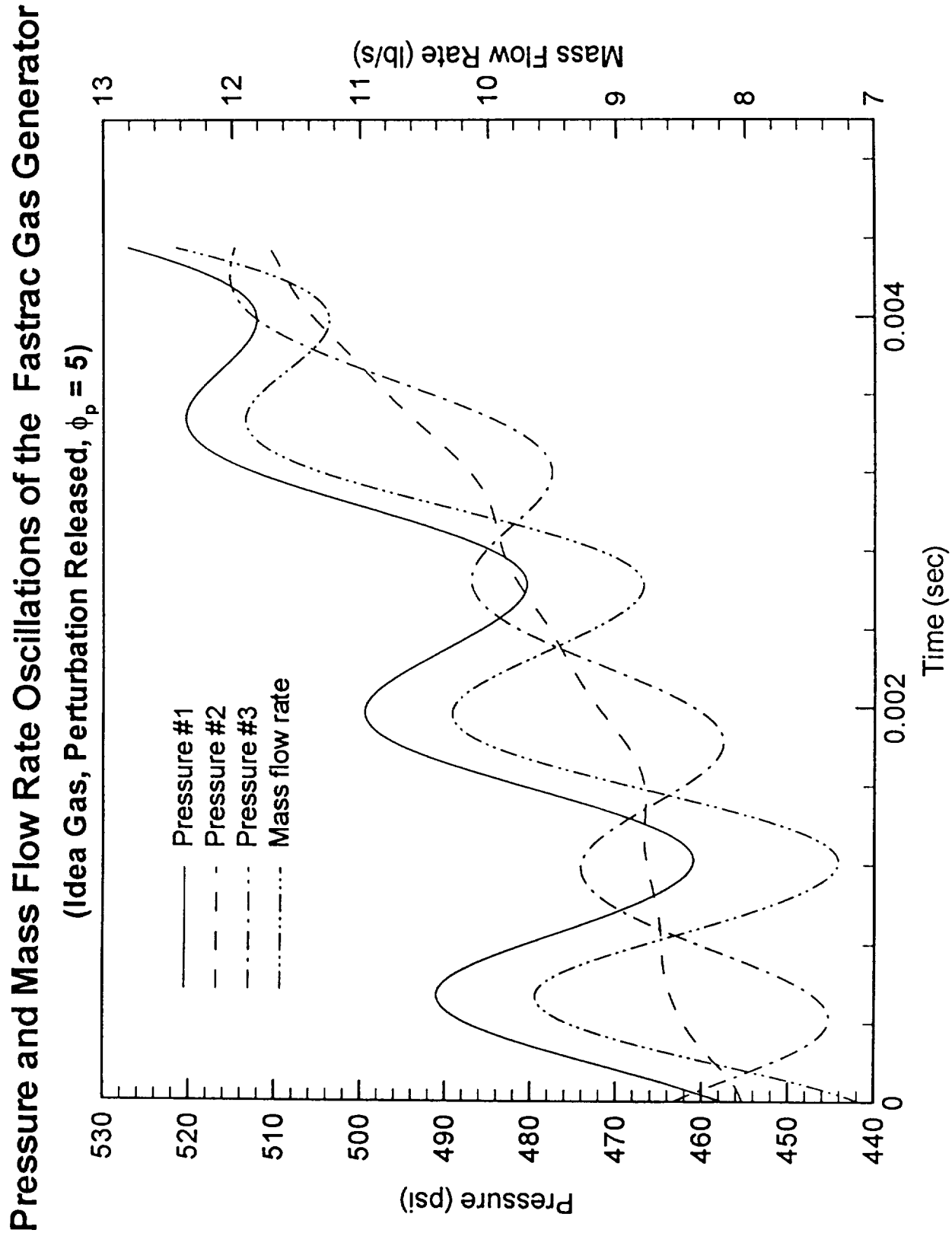
Pressure and Mass Flow Rate Oscillations of the Fastrac Gas Generator
(Idea Gas, Perturbation Released, ϕ_p = 5)
Pressure #1
Pressure #2
Pressure #3
Mass flow rate
Pressure (psi)
Mass Flow Rate (lb/s)
Time (sec)
530
520
510
500
490
480
470
460
450
440
13
12
11
10
9
8
7
0
0.002
0.004

Figure 13

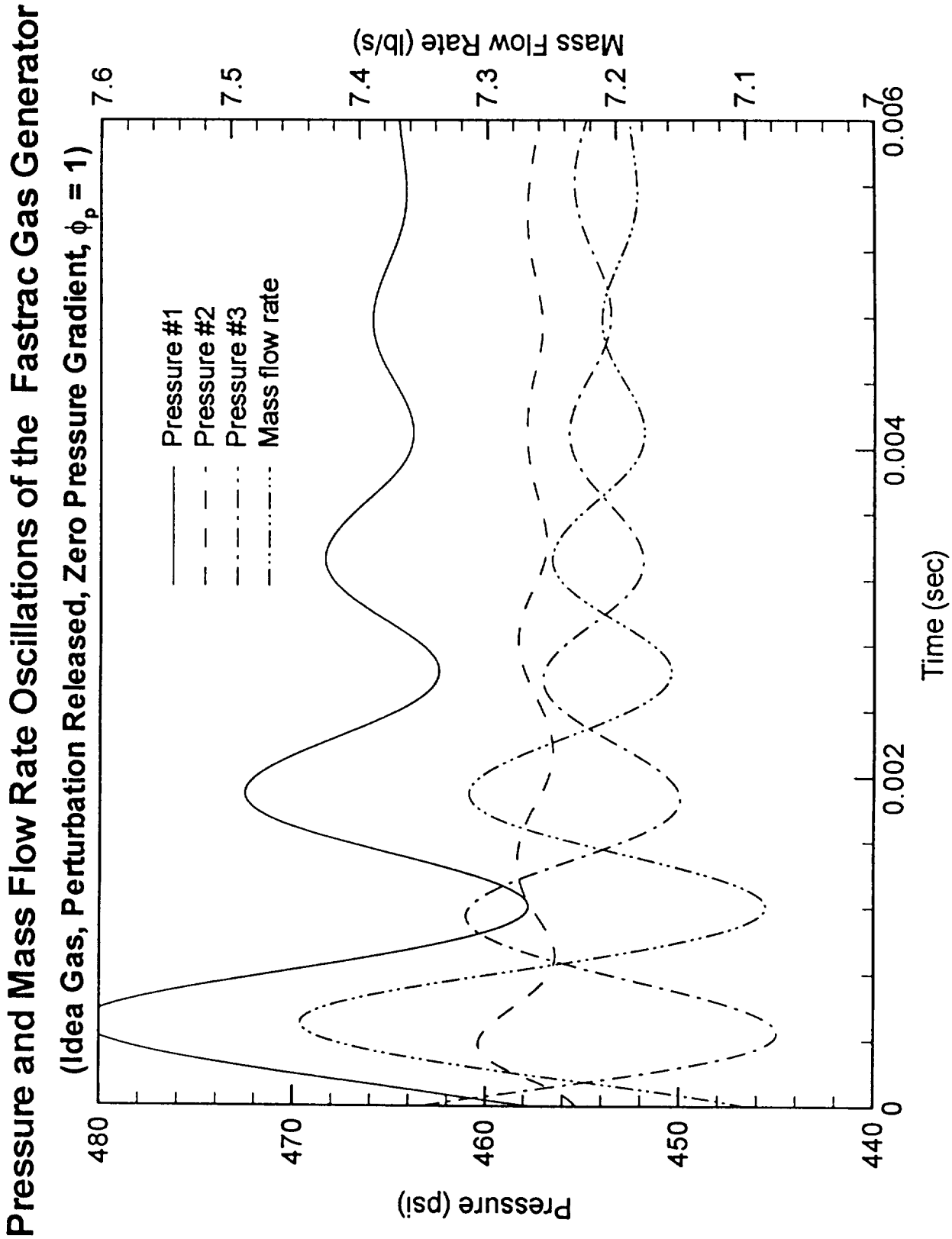
Pressure and Mass Flow Rate Oscillations of the Fastrac Gas Generator
(Idea Gas, Perturbation Released, Zero Pressure Gradient, ϕ_p = 1)
Pressure #1
Pressure #2
Pressure #3
Mass flow rate
Pressure (psi)
Mass Flow Rate (lb/s)
Time (sec)
480
470
460
450
440
7.6
7.5
7.4
7.3
7.2
7.1
7
0
0.002
0.004
0.006

Figure 14

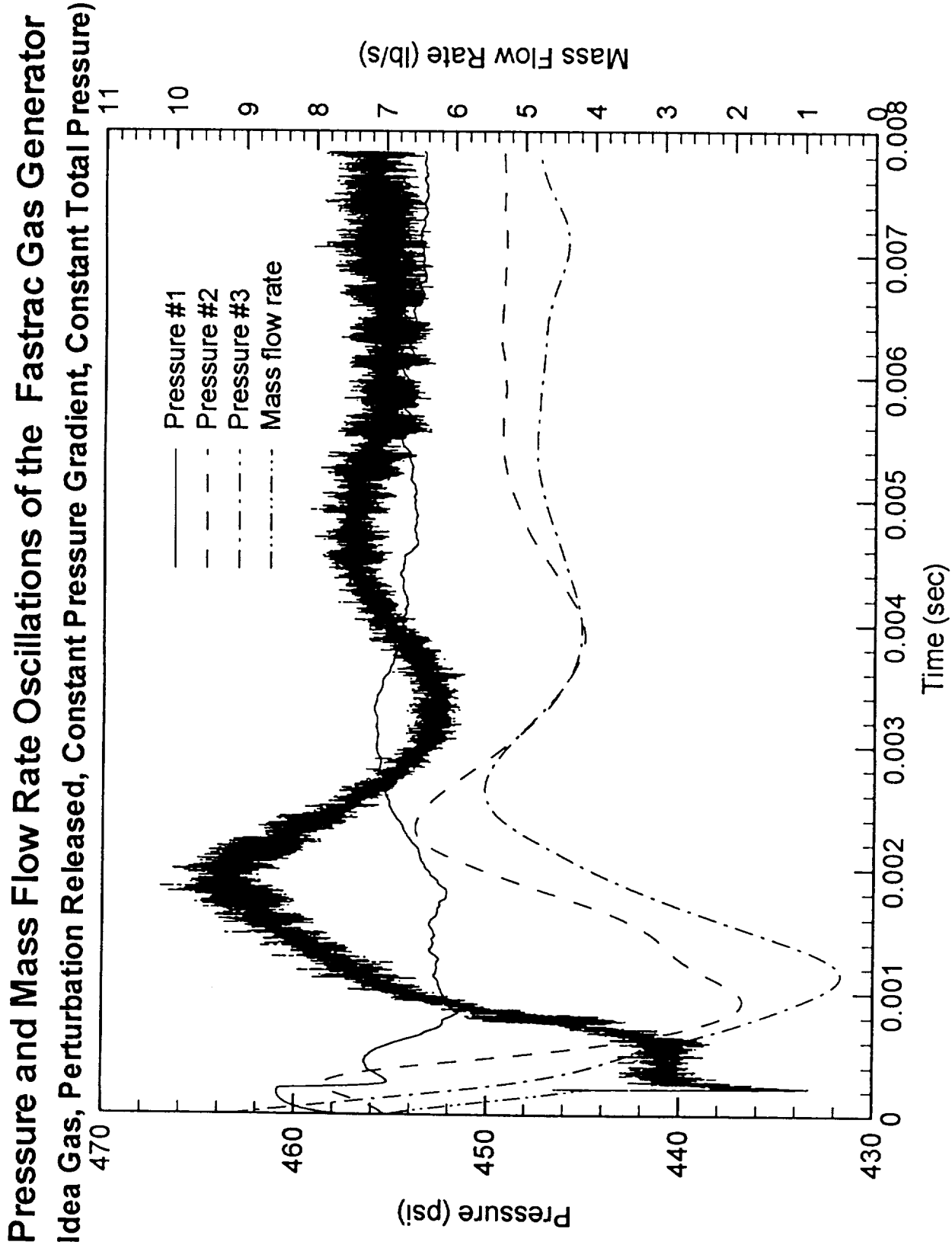
Pressure and Mass Flow Rate Oscillations of the Fastrac Gas Generator
(Idea Gas, Perturbation Released, Constant Pressure Gradient, Constant Total Pressure)
Pressure #1
Pressure #2
Pressure #3
Mass flow rate
Pressure (psi)
Mass Flow Rate (lb/s)
Time (sec)
470
460
450
440
430
11
10
9
8
7
6
5
4
3
2
1
0
0
0.001
0.002
0.003
0.004
0.005
0.006
0.007
0.008

Figure 15

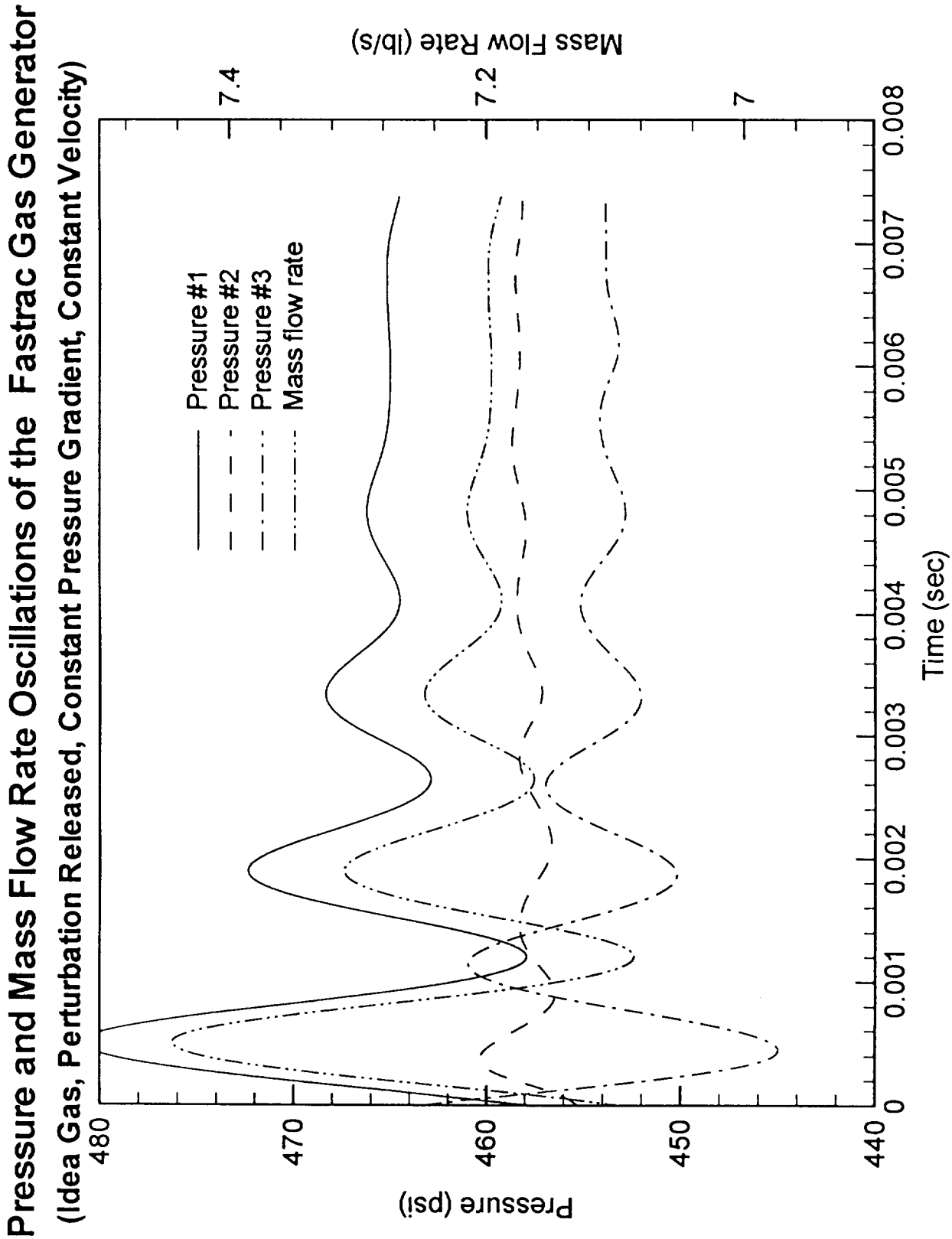
Pressure and Mass Flow Rate Oscillations of the Fastrac Gas Generator
(Idea Gas, Perturbation Released, Constant Pressure Gradient, Constant Velocity)
Pressure #1
Pressure #2
Pressure #3
Mass flow rate
Pressure (psi)
Mass Flow Rate (lb/s)
Time (sec)
480
470
460
450
440
7.4
7.2
7
0
0.001
0.002
0.003
0.004
0.005
0.006
0.007
0.008

Figure 16

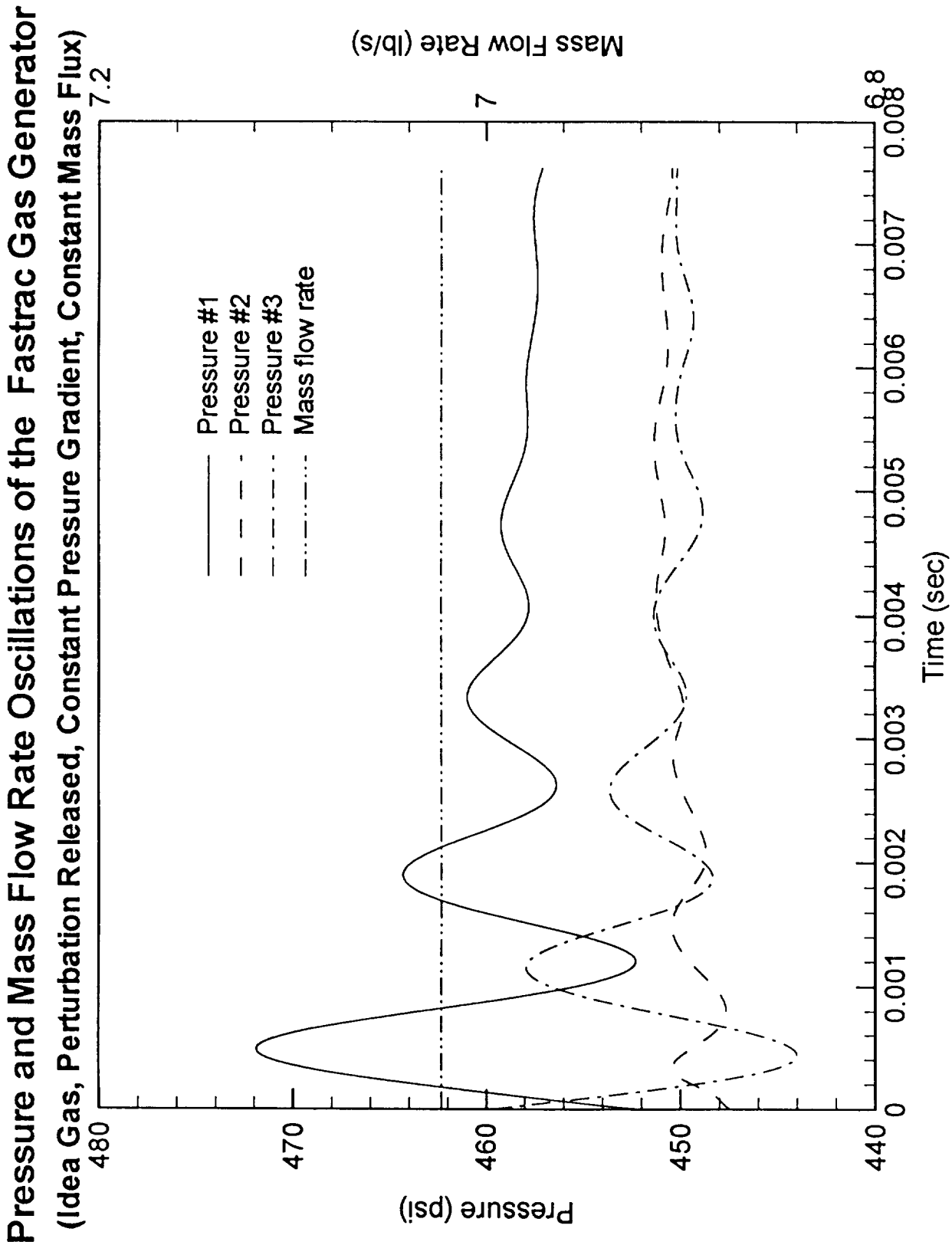
Pressure and Mass Flow Rate Oscillations of the Fastrac Gas Generator
(Idea Gas, Perturbation Released, Constant Pressure Gradient, Constant Mass Flux)
Pressure #1
Pressure #2
Pressure #3
Mass flow rate
Pressure (psi)
Mass Flow Rate (lb/s)
Time (sec)
480
470
460
450
440
7.2
7
6.8
0
0.001
0.002
0.003
0.004
0.005
0.006
0.007
0.008

REPORT DOCUMENTATION PAGE

Form Approved
OMB No. 0704-0188

1. AGENCY USE ONLY *(Leave blank)*	2. REPORT DATE	3. REPORT TYPE AND DATES COVERED
	June 9, 2000	

4. TITLE AND SUBTITLE

Quantifying Instability Sources in Liquid Rocket Engines

5. FUNDING NUMBERS

NAS8-00070

6. AUTHORS

Richard C. Farmer

7. PERFORMING ORGANIZATION NAME(S) AND ADDRESS(ES)

SECA, Inc.
3313 Bob Wallace Avenue, Suite 201
Huntsville, AL 35805

8. PERFORMING ORGANIZATION REPORT NUMBER

SECA-FR-00-04

9. SPONSORING/MONITORING AGENCY NAME(S) AND ADDRESS(ES)

NASA/MSFC
Marshall Space Flight Center, AL 35812

10. SPONSORING/MONITORING AGENCY REPORT NUMBER

11. SUPPLEMENTARY NOTES

12a. DISTRIBUTION/AVAILABILITY STATEMENT

12b. DISTRIBUTION CODE

13. ABSTRACT *(Maximum 200 words)*

Computational fluid dynamics methodology to predict the effects of combusting flows on acoustic pressure oscillations in liquid rocket engines (LREs) is under development. The intent of the investigation is to develop the causal physics of combustion driven acoustic resonances in LREs. The crux of the analysis is the accurate simulation of pressure/density/sound speed in a combustor which when used by the FDNS-RFV CFD code will produce realistic flow phenomena. An analysis of a gas generator considered for the Fastrac engine will be used as a test validation case.

14. SUBJECT TERMS	15. NUMBER OF PAGES
	25
	16. PRICE CODE

17. SECURITY CLASSIFICATION OF REPORT	18. SECURITY CLASSIFICATION OF THIS PAGE	19. SECURITY CLASSIFICATION OF ABSTRACT	20. LIMITATION OF ABSTRACT